# Supporting Information for

# Interfacial Linkages Enhance Redox-Adaptive Bifunctional Catalysis of Heterostructured Catalysts

***Yu-Xinag Lin,[a] Yu-Chieh Ting,[a] Chiung-Wen Chang,[a] Shao-I Chang,[a] Kai-An Lee,[a] Tsung-Wei Hsueh,[a] Chia-Hsien Lin,[a] Shih-Yuan Lu[a]****

***Affiliations:***

Department of Chemical Engineering, National Tsing Hua University, Hsinchu 300044, Taiwan.

***Email: sylu@mx.nthu.edu.tw (Shih-Yuan Lu)**

**Keywords:** Water Electrolysis, Layered Double Hydroxide, Oxygen Bridged Interfacial Linkage, Heterostructured Catalyst, Bifunctional Catalyst

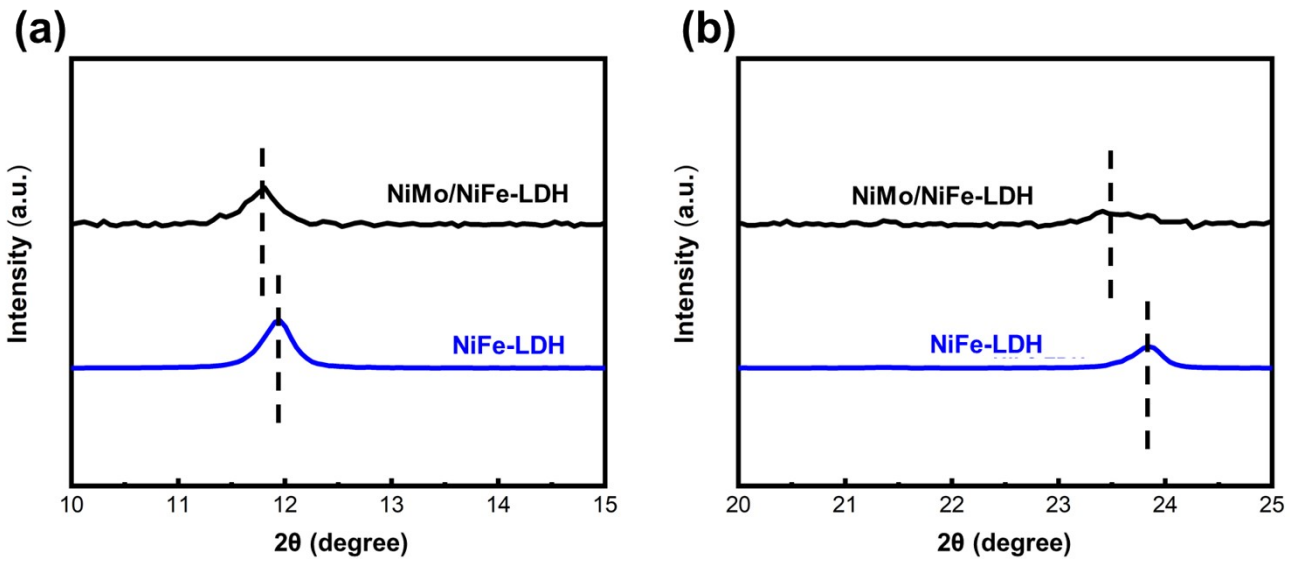


**Figure S1**. Locally enlarged diffraction peaks of (a) (003) and (b) (006) of NiMo/NiFe-LDH and NiFe-LDH for comparison.

**Table S1.** Elemental compositions of NiFe-LDH, NiMo, and NiMo/NiFe-LDH determined with ICP-OES.

| Sample | Ni (at%) | Fe (at%) | Mo (at%) |
|---|---|---|---|
| NiFe-LDH | 65.23 | 34.77 | 0 |
| NiMo | 60.66 | 0 | 39.34 |
| NiMo/NiFe-LDH | 66.69 | 32.1 | 1.21 |

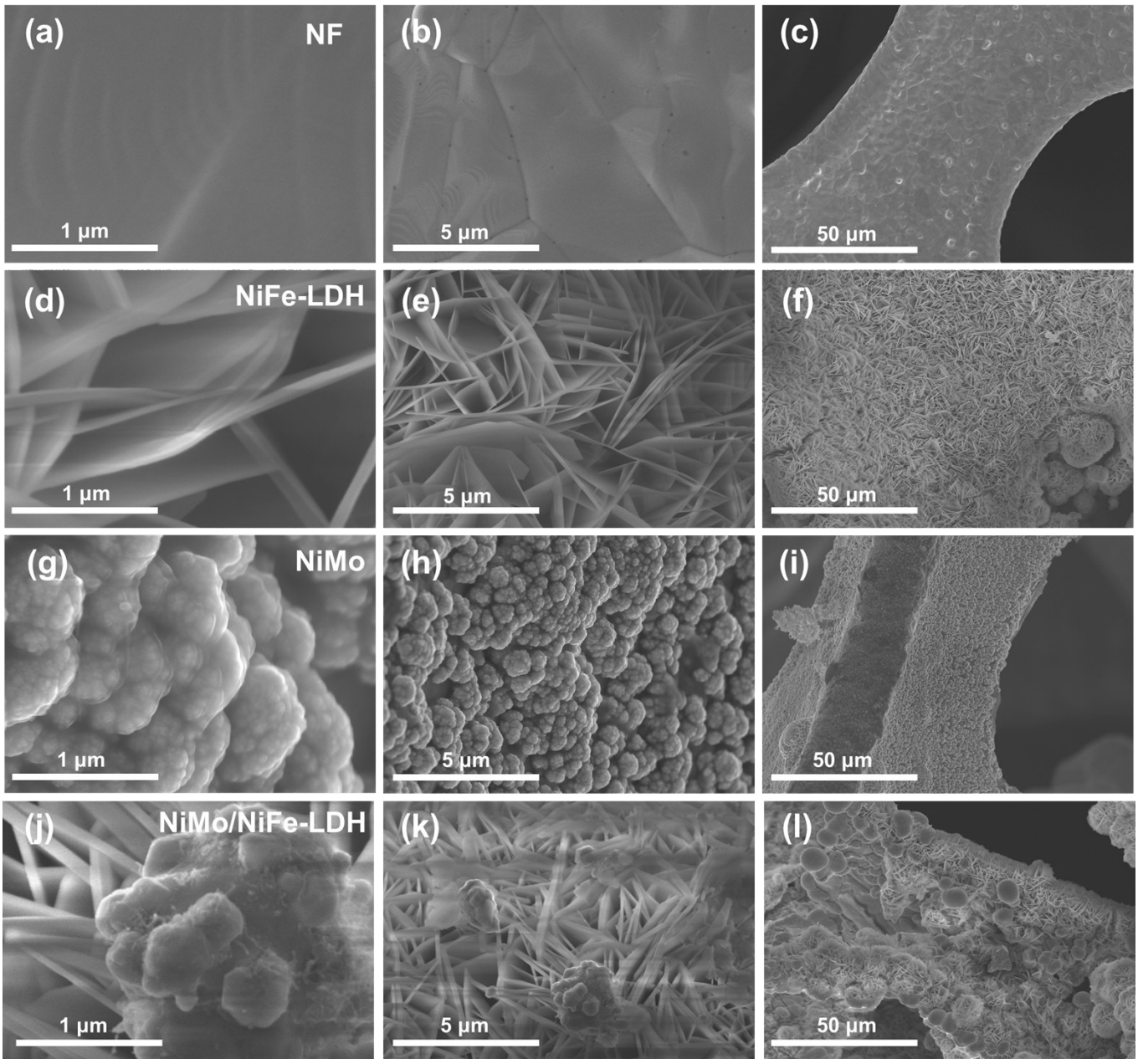


**Figure S2**. SEM images of (a-c) NF, (d-f) NiFe-LDH on NF, (g-i) NiMo on NF, and (j-l) NiMo/NiFe-LDH on NF at decreasing magnifications.

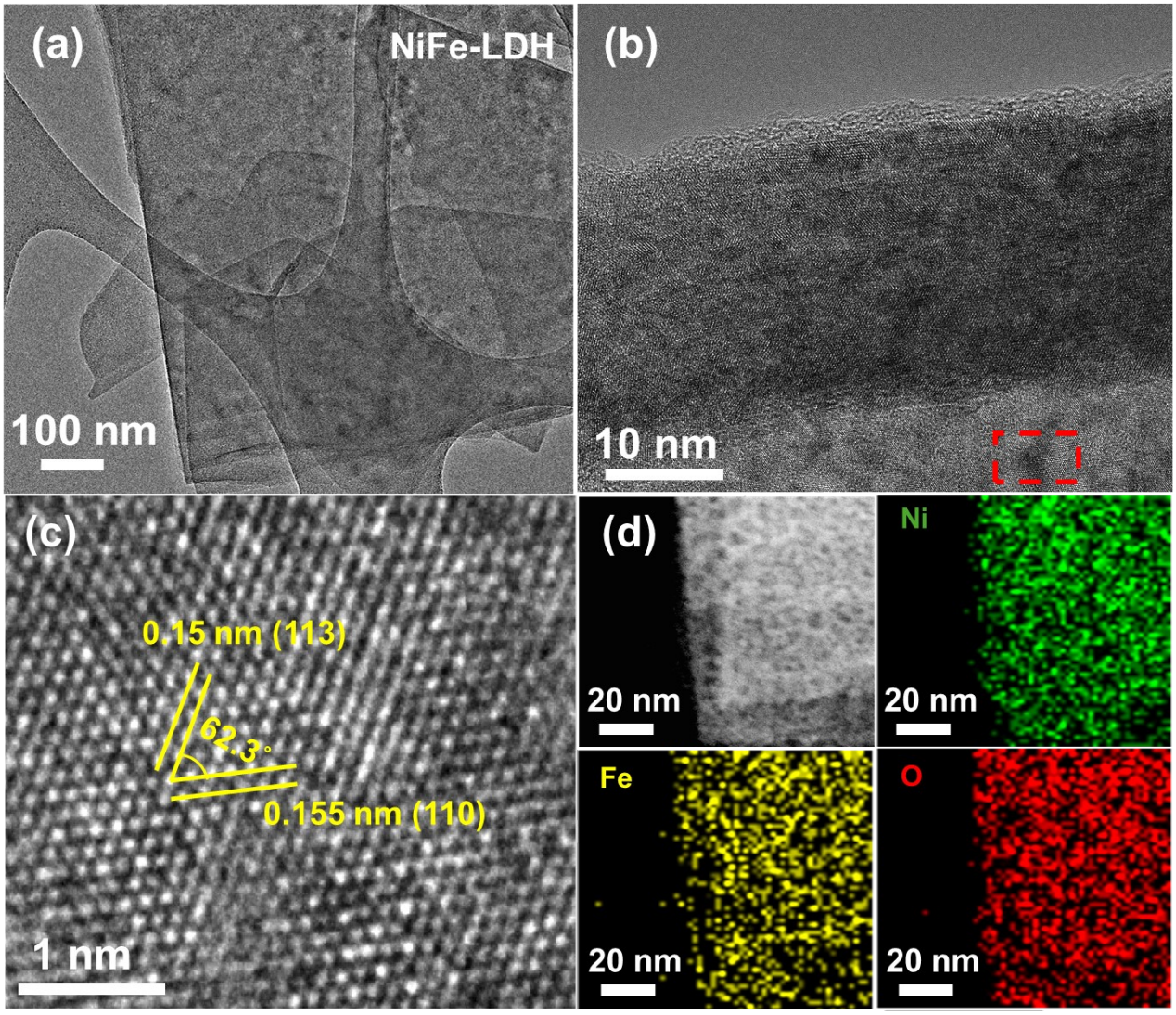


**Figure S3.** (a) TEM image of NiFe-LDH. (b) HRTEM image of NiFe-LDH. (c) Locally enlarged HRTEM image of NiFe-LDH with exposed facets designated. (c) HAADF-STEM image of NiFe-LDH with corresponding EDS elemental mapping of Ni, Fe, and O.

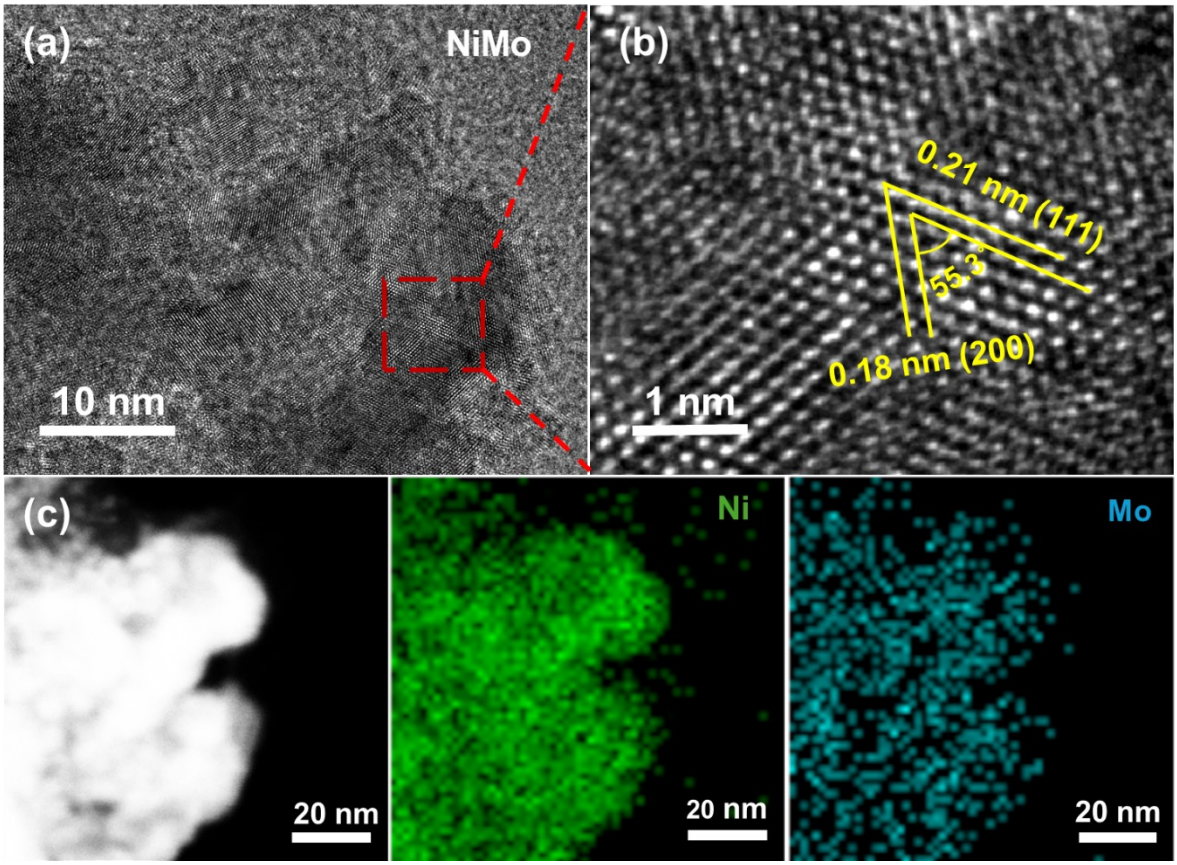


**Figure S4.** (a) HR-TEM image of NiMo. (b) Locally enlarged HRTEM image of NiMo with exposed facets designated. (c) HAADF-STEM image of NiMo with corresponding EDS elemental mapping of Ni and Mo.

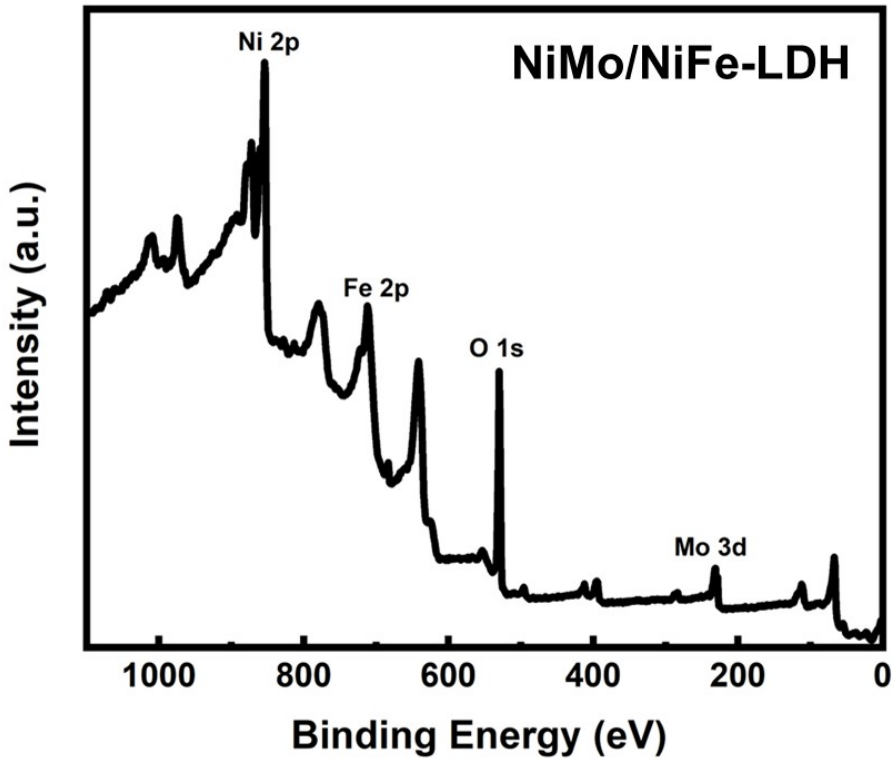


**Figure S5.** XPS survey spectrum of NiMo/NiFe-LDH.

**Table S2.** Binding energies (in eV) of constituent peaks for HRXPS spectra of Ni 2p of NiFe-LDH, NiMo, and NiMo/NiFe-LDH.

| Catalyst | | $Ni^0$ | $Ni^{2+}$ | Ni sat. |
|---|---|---|---|---|
| NiFe-LDH | Ni $2p_{3/2}$ | | 855.7 | 861.4 |
| | Ni $2p_{1/2}$ | | 873.5 | 879.7 |
| NiMo | Ni $2p_{3/2}$ | 853.0 | | 859.4 |
| | Ni $2p_{1/2}$ | 870.2 | | |
| NiMo/NiFe-LDH | Ni $2p_{3/2}$ | 853.3 | 855.5 | 860.4 |
| | Ni $2p_{1/2}$ | 870.3 | 872.7 | 878.7 |

**Table S3.** Binding energies (in eV) of constituent peaks for HRXPS spectra of Fe 2p of NiFe-LDH and NiMo/NiFe-LDH.

| Catalyst | | $Fe^{3+}$ | Fe sat. |
|---|---|---|---|
| NiFe-LDH | $Fe\ 2p_{3/2}$ | 711.1 | 714.0 |
| | $Fe\ 2p_{1/2}$ | 724.9 | |
| NiMo/NiFe-LDH | $Fe\ 2p_{3/2}$ | 710.8 | 713.8 |
| | $Fe\ 2p_{1/2}$ | 723.9 | |

**Table S4.** Binding energies (in eV) of constituent peaks for HR-XPS spectra of Mo 3d of NiMo and NiMo/NiFe-LDH.

| Catalyst | | $Mo^0$ | $Mo^{4+}$ | $Mo^{6+}$ |
|---|---|---|---|---|
| NiMo | Mo $3d_{5/2}$ | 228.1 | 229.5 | 232.0 |
| | Mo $3d_{3/2}$ | 231.1 | 233.2 | 235.3 |
| NiMo/NiFe-LDH | Mo $3d_{5/2}$ | 228.3 | 229.7 | 232.1 |
| | Mo $3d_{3/2}$ | 231.2 | 233.4 | 235.4 |

**Table S5.** Binding energies (in eV) of constituent peaks for HR-XPS spectra of O 1s of NiFe-LDH and NiMo/NiFe-LDH.

| Catalyst | | M-O | $OH^-$ | $H_2O_{(ad)}$ |
|---|---|---|---|---|
| NiFe-LDH | O 1s | 529.8 | 531.0 | 532.6 |
| NiMo/NiFe-LDH | O 1s | 529.6 | 531.0 | 532.5 |

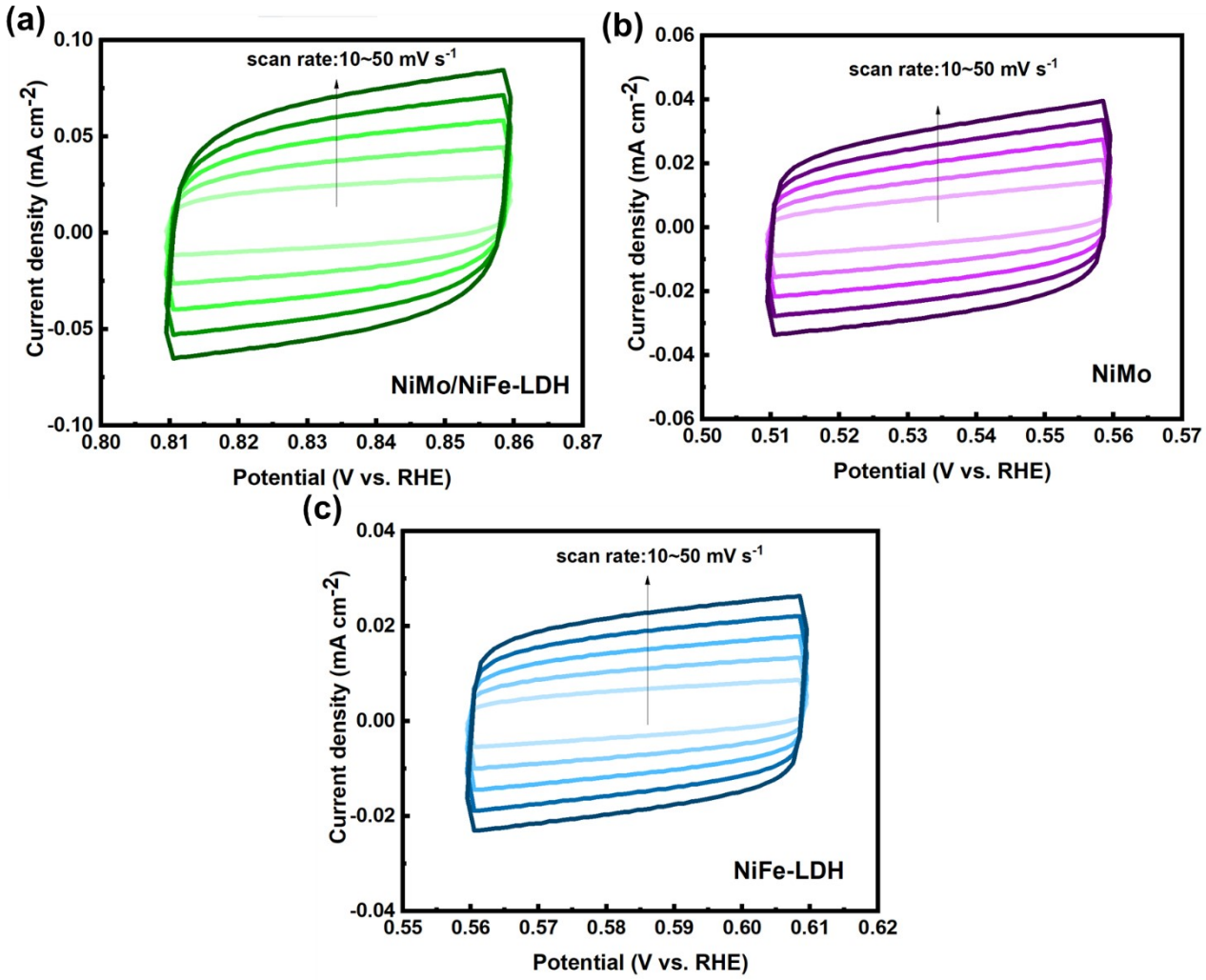


**Figure S6.** CV curves of (a) NiMo/NiFe-LDH, (b) NiMo, and (c) NiFe-LDH in non-Faradaic potential windows recorded at increasing scan rates from 10 to 50 mV $s^{-1}$.

**Table S6.** Fitted $R_{ct}$ values (Ω) for NiFe-LDH, NiMo, and NiMo/NiFe-LDH under (a) HER (-0.3 V) and (b) OER (1.56 V) conditions.

| **HER** | | **OER** | |
|---|---|---|---|
| catalyst | $R_{ct}$ (Ω) | catalyst | $R_{ct}$ (Ω) |
| NiMo/NiFe-LDH | 1.72 | NiMo/NiFe-LDH | 0.42 |
| NiMo | 2.48 | NiMo | 3.9 |
| NiFe-LDH | 4.6 | NiFe-LDH | 0.82 |

**Table S7.** Comparison of HER, OER, and overall water splitting (OWS) performances of NiMo/NiFe-LDH with those of recently reported LDH/ alloy based heterostructured catalysts.

| HER | | | OER | | | OWS $\eta_{10}$ (V) | Ref |
|---|---|---|---|---|---|---|---|
| **Catalyst** | **Overpotential $\eta_{10}$ (mV)** | **Tafel slope (mV dec$^{-1}$ )** | **Catalyst** | **Overpotential $\eta_{10}$ (mV)** | **Tafel slope (mV dec$^{-1}$ )** | | |
| NiMo/NiFe-LDH | 40 | 73 | NiMo/NiFe-LDH | 190 | 38 | 1.476 | This work |
| CoNiN@NiFe-LDH | 150 | 169 | CoNiN@NiFe LDH | 227 | 58 | 1.63 | [S1] |
| NiFe-LDH@NiCoP | 120 | 88 | NiFe LDH@NiCoP | 220 | 49 | 1.57 | [S2] |
| NiCu@NiFe-LDH | 85 | 92 | NiCu@NiFe LDH | 244 | 51 | 1.54 | [S3] |
| $MoS_2$/NiFe-LDH | 98 | 98 | $MoS_2$/NiFe LDH | 257 | 59 | 1.61 | [S4] |
| NiMo/$NiCo_2O_4$ | 44 | 61 | NiMo/$NiCo_2O_4$ | 305 | 73 | 1.54 | [S5] |
| NiS/NiMo | 77 | 95 | NiS/NiMo | 245 | 87 | 1.58 | [S6] |
| Cu-NiCo LDH@CC | 73 | 79 | Cu-NiCo LDH@CC | 151 | 68 | 1.51 | [S7] |
| NiTe@CoFe LDH | 103 | 100 | NiTe@CoFe LDH | 218 | 20 | 1.56 | [S8] |
| CuNi/CoFe LDH@NF | 56 | 34 | CuNi/CoFe LDH@NF | 268($\eta_{50}$) | 63 | 1.49 | [S9] |

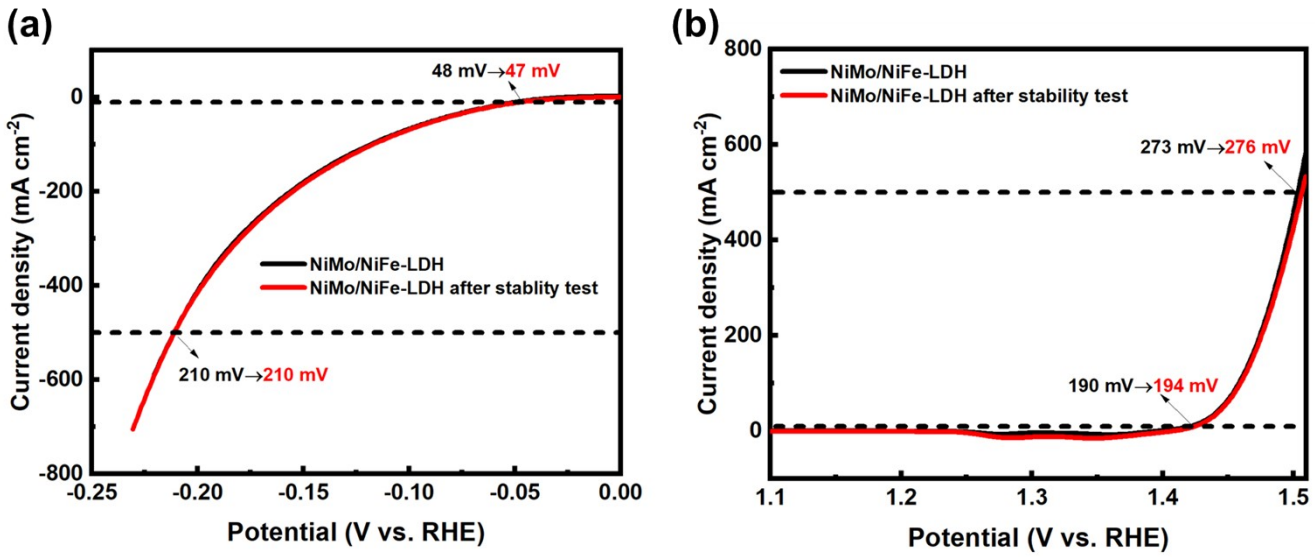


**Figure S7.** Comparison of (a) HER and (b) OER LSV curves before and after long-term stability tests (500 mA $cm^{-2}$, 65 h) for NiMo/NiFe-LDH.

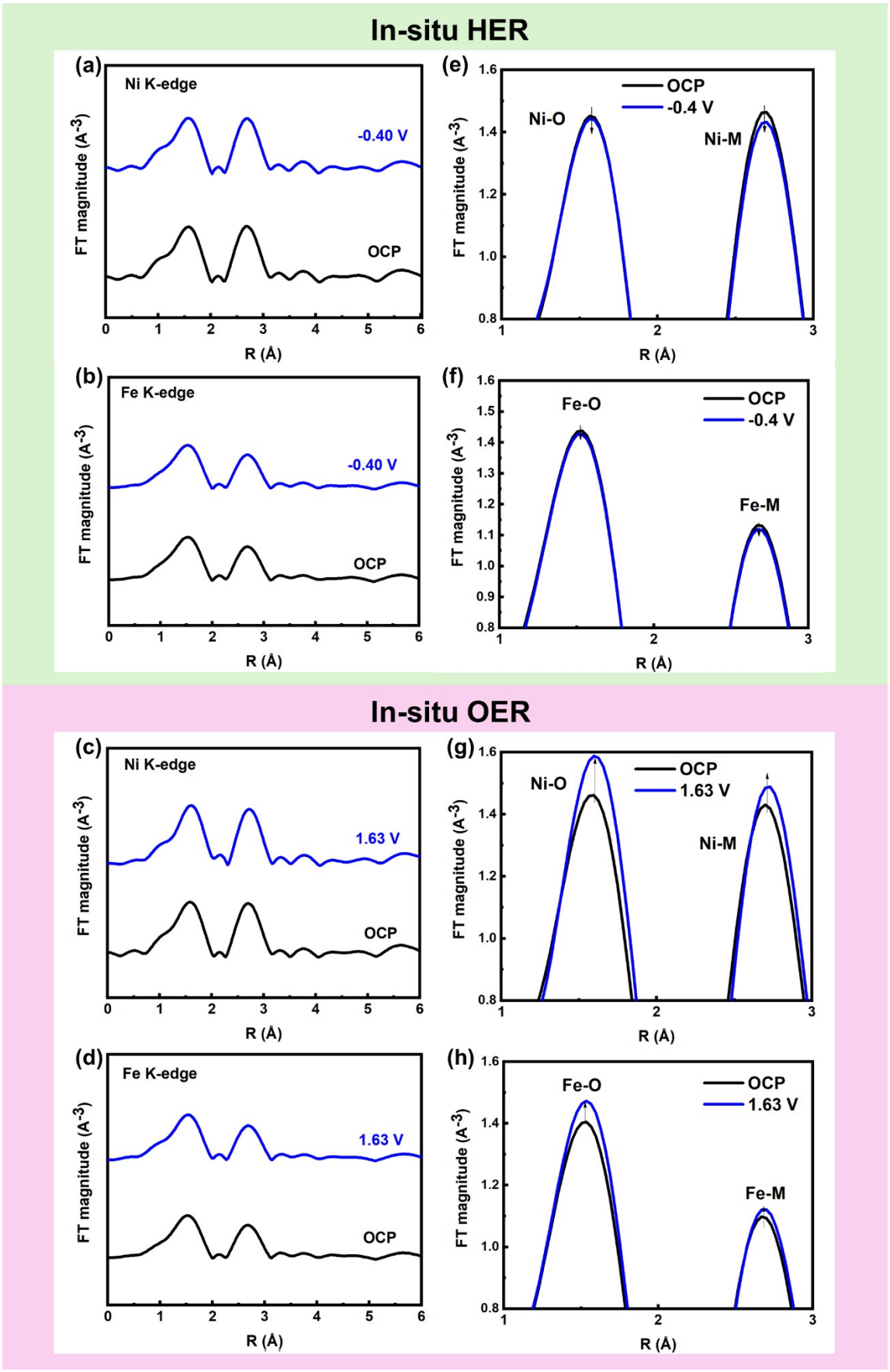


**Figure S8.** k²-weighted in-situ FT-EXAFS spectra of NiMo/NiFe-LDH under HER conditions at (a) Ni K-edge and (b) Fe K-edge, and under OER conditions at (c) Ni K-edge and (d) Fe K-edge, with corresponding locally enlarged overlaid curves presented in panels (e), (f), (g), and (h), respectively.

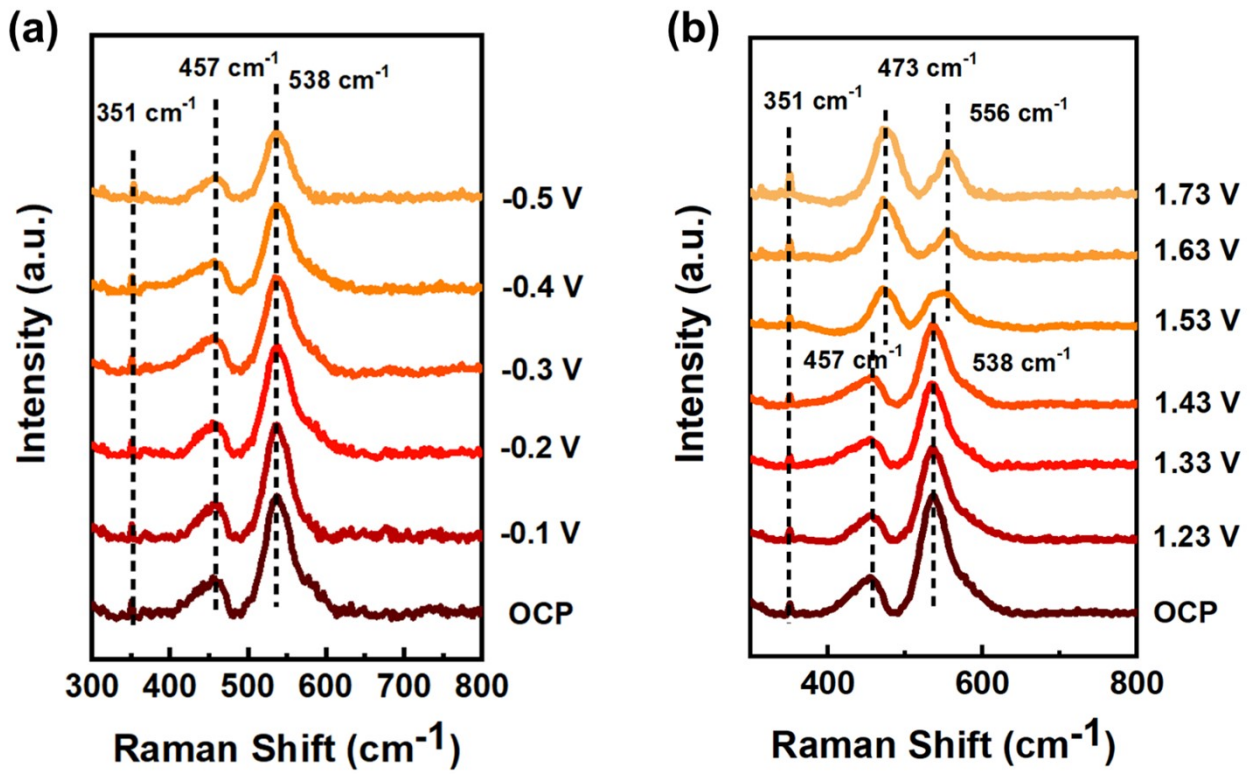


**Figure S9.** In-situ Raman spectra of NiMo/NiFe-LDH under (a) HER conditions and (b) OER conditions.

## References


[S1] J. Wang, G. Lv, C. Wang, A highly efficient and robust hybrid structure of CoNiN@NiFe LDH for overall water splitting by accelerating hydrogen evolution kinetics on NiFe LDH, Applied Surface Science 570 (2021). https://doi.org/10.1016/j.apsusc.2021.151182.

[S2] H. Zhang, X. Li, A. Hähnel, V. Naumann, C. Lin, S. Azimi, S.L. Schweizer, A.W. Maijenburg, R.B. Wehrspohn, Bifunctional Heterostructure Assembly of NiFe LDH Nanosheets on NiCoP Nanowires for Highly Efficient and Stable Overall Water Splitting, Advanced Functional Materials 28(14) (2018). https://doi.org/10.1002/adfm.201706847.

[S3] H. Su, J. Jiang, N. Li, Y. Gao, L. Ge, NiCu alloys anchored defect-rich NiFe layered double-hydroxides as efficient electrocatalysts for overall water splitting, Chemical Engineering Journal 446 (2022). https://doi.org/10.1016/j.cej.2022.137226.

[S4] X.-P. Li, L.-R. Zheng, S.-J. Liu, T. Ouyang, S. Ye, Z.-Q. Liu, Heterostructures of NiFe LDH hierarchically assembled on MoS2 nanosheets as high-efficiency electrocatalysts for overall water splitting, Chinese Chemical Letters 33(11) (2022) 4761-4765. https://doi.org/10.1016/j.cclet.2021.12.095.

[S5] H. Chen, S. Qiao, J. Yang, X. Du, NiMo/NiCo2O4 as synergy catalyst supported on nickel foam for efficient overall water splitting, Molecular Catalysis 518 (2022). https://doi.org/10.1016/j.mcat.2021.112086.

[S6] T. Ren, X. Huang, J. Chen, G. Wang, Y. Liu, F. Bao, W. Guo, Surface-sulphurated nickel–molybdenum alloy film as enhanced electrocatalysts for alkaline overall water splitting, International Journal of Hydrogen Energy 57 (2024) 983-989. https://doi.org/10.1016/j.ijhydene.2024.01.077.

[S7] X. Xia, S. Wang, D. Liu, F. Wang, X. Zhang, H. Zhang, X. Yu, Z. Pang, G. Li, C. Chen, Y. Zhao, L. Ji, Q. Xu, X. Zou, X. Lu, Electronic Modulation in Cu Doped NiCo LDH/NiCo Heterostructure for Highly Efficient Overall Water Splitting, Small 20(28) (2024) e2311182. https://doi.org/10.1002/smll.202311182.

[S8] L. Yao, R. Li, H. Zhang, M. Humayun, X. Xu, Y. Fu, A. Nikiforov, C. Wang, Interface engineering of NiTe@CoFe LDH for highly efficient overall water-splitting, International Journal of Hydrogen Energy 47(76) (2022) 32394-32404. https://doi.org/10.1016/j.ijhydene.2022.07.135.

[S9] D. Wang, Y. Chu, Y. Wu, M. Zhu, L. Pan, R. Li, Y. Chen, W. Wang, N. Mitsuzaki, Z. Chen, Synergistic coupling of a CuNi alloy with a CoFe LDH heterostructure on nickel foam toward high-efficiency overall water splitting, Journal of Materials Chemistry A 12(48) (2024) 33680-33688. https://doi.org/10.1039/d4ta05681g.